AIAA JOURNAL
Vol. 44, No. 7, July 2006

Wall Pressure and Shear Stress Spectra from Direct Simulations of Channel Flow

Z. W. Hu,* C. L. Morfey,† and N. D. Sandham‡
University of Southampton, Southampton, SO17 1BJ England, United Kingdom

DOI: 10.2514/1.17638

Wall pressure and shear stress spectra from direct numerical simulations of turbulent plane channel flow are presented in this paper. Simulations have been carried out at a series of Reynolds numbers up to $Re_\tau = 1440$, which corresponds to $Re = 6.92 \times 10^4$ based on channel width and centerline velocity. Single-point and two-point statistics for velocity, pressure, and their derivatives have been collected, including velocity moments up to fourth order.§ The results have been used to study the Reynolds number dependence of wall pressure and shear stress spectra. It is found that the point spectrum of wall pressure collapses for $Re_\tau \geq 360$ under a mixed scaling for frequencies lower than the peak frequency of the frequency-weighted spectrum, and under viscous scaling for frequencies higher than the peak. Point spectra of wall shear stress components are found to collapse for $Re_\tau \geq 360$ under viscous scaling. The normalized mean square wall pressure increases linearly with the logarithm of Reynolds number. The rms wall shear stresses also increase with Reynolds number over the present range, but suggest some leveling off at high Reynolds number.

I. Introduction

BECAUSE wall pressure and wall shear stress fluctuations in wall-bounded turbulent flows are sources of structural vibration and sound radiation, their spectra are needed for engineering predictions. Several experimental investigations [1–5] have been carried out for the fluctuating wall pressure, and the Reynolds number dependence of measured point spectra has been studied. It has been shown that there is no universal scaling law to collapse the whole range of frequencies. Viscous scaling is generally used for the high-frequency end, whereas outer scaling and mixed scaling have also been tried for the low and midfrequency ranges.

Fluctuating wall shear stresses are more difficult to measure than pressure. The only direct way is to measure the instantaneous lateral force on a very small area of the wall. Data from indirect measurement techniques, such as measuring the velocity fluctuation in the near wall region (viscous sublayer), are influenced by the probe disturbance and by spatial averaging over the finite probe size, especially at high Reynolds number. Sensor calibration also influences the measured results. Although MEMS (micro-electro-mechanical system) based sensors, with their highly integrated fabrication, have performed well in measuring pressure fluctuations their accuracy for wall shear stress measurements still needs improving, as was summarized in the review of Löfdahl [6]. These experimental difficulties cause large data scatter, as demonstrated by Alfredsson et al. [7] who assembled the available root-mean-square (rms) wall shear stress measurements from different investigators. It is therefore difficult to use experimental data to find the best scaling law for wall shear stress spectra. For example, Keith and Bennett [8] found that experimental uncertainties made it impossible to decide whether inner or outer scaling is more effective in collapsing the measured spectra.

With the help of supercomputers, direct numerical simulations (DNS) can now be performed at moderate Reynolds number for simple flow geometry. Turbulent Poiseuille flow in a plane channel is a well-defined problem, suitable for DNS with periodic boundary conditions in the streamwise and spanwise directions. Kim et al. [9] (referred to as KMM hereafter) first carried out DNS for turbulent channel flow at a Reynolds number $Re_\tau = 180$ based on friction velocity and channel half-width, whereas Moser et al. [10] (referred to as MKM hereafter) extended the Reynolds number range to $Re_\tau = 590$. Del Alamo et al. [11] performed channel flow DNS in large computational boxes for $Re_\tau = 547$ and 934, and also ran simulations in a small box up to $Re_\tau = 1900$ to study the scaling of energy containing structures. DNS of channel flow has also been used to study wall pressure and shear stress fluctuations. For example, wall pressure and shear stress spectra obtained from channel flow DNS at $Re_\tau = 180$ have been compared with available experimental measurements [12,13]. Hu et al. [14,15] used wave-number–frequency spectra data from an earlier calculation ($Re_\tau \leq 360$) to study the low-wave-number behavior of wall pressure and shear stresses. Simulations of Abe et al. [16] for channel flow up to $Re_\tau = 640$ studied the influence of large scale structures on wall shear stresses.

In the present contribution, DNS calculations have been performed for a series of Reynolds numbers up to $Re_\tau = 1440$, which corresponds to $Re = 6.92 \times 10^4$ based on channel width and centerline velocity. Point spectra of wall pressure and wall shear stress are calculated from wave-number–frequency spectra in the DNS database and are compared with experimental data. The database from current simulations extended the Reynolds number range of the previous study of Hu et al., [14,15] thus permitting Reynolds number trends to be studied. The Reynolds number dependence of rms wall pressure and shear stress (both streamwise and spanwise components) is also presented.

II. DNS of Incompressible Plane Channel Flow

A. Spectral Method for DNS

The incompressible continuity and momentum equations are nondimensionalized for turbulent Poiseuille flow with channel half-width h^* as the reference length and friction velocity u_τ^* as the reference velocity, giving the following nondimensional form:

Received 11 May 2005; revision received 6 January 2006; accepted for publication 13 February 2006.

*Senior Research Fellow, Aerodynamics & Flight Mechanics Research Group, School of Engineering Sciences.

†Professor, Fluid Dynamics and Acoustics Group, ISVR.

‡Professor, Aerodynamics & Flight Mechanics Research Group, School of Engineering Sciences, Senior Member AIAA.

§Data available on-line at http://www.dnsdata.afm.ses.soton.ac.uk/ [cited 16 November 2004].

$$\frac{\partial u_j}{\partial x_j} = 0 \tag{1}$$

$$\frac{\partial u_i}{\partial t} = \epsilon_{ijk} u_j \omega_k + \delta_{1i}\Lambda - \frac{\partial \Pi}{\partial x_i} + \frac{1}{Re_\tau}\frac{\partial^2 u_i}{\partial x_j \partial x_j} \tag{2}$$

where the Reynolds number is $Re_\tau = u_\tau^* h^*/\nu^*$, with ν^* being the kinematic viscosity. $\Pi = p + u_i u_i/2$ is the modified pressure, ϵ_{ijk} is the permutation tensor, and $\omega_k = \epsilon_{ijk}\partial u_j/\partial x_i$ is the vorticity.

Poiseuille flow is driven by a mean pressure gradient, whose nondimensional value Λ is equal to 1. The channel coordinates are $x_1 = x$ in the streamwise direction, $x_2 = y$ in the spanwise direction, and $x_3 = z$ in the wall-normal direction, with the channel walls at $z = \pm 1$. (u, v, w) denote the nondimensional velocities in the (x, y, z) directions.

The spectral method of Kleiser and Schumann [17] has been used to solve the incompressible governing equations with Fourier discretization applied to the two periodic directions (x, y), and Chebyshev polynomial expansion to the wall-normal direction z. In the periodic directions a twofold discrete Fourier transformation is carried out for any quantity q by the following forward and backward transforms:

$$\tilde{q}(k_{xl}, k_{ym}) = \frac{1}{N_y}\sum_{j=0}^{N_y-1}\left\{\frac{1}{N_x}\sum_{i=0}^{N_x-1} q(x_i, y_j)\exp(-ik_{xl}x_i)\right\} \times \exp(-ik_{ym}y_j) \tag{3}$$

$$q(x_i, y_j) = \tilde{q}(0, y_j) + 2\sum_{l=1}^{N_x/2}\left\{\sum_{m=-N_y/2}^{N_y/2}\tilde{q}(k_{xl}, k_{ym})\exp(ik_{ym}y_j)\right\} \times \exp(ik_{xl}x_i) \tag{4}$$

where $i = \sqrt{-1}$. $k_{xl} = 2\pi l/L_x (0 \le l \le N_x/2)$ and $k_{ym} = 2\pi m/L_y (-N_y/2 \le m \le N_y/2)$ are wave numbers in the x and y directions, respectively. The grid coordinates are uniform in the streamwise and spanwise directions with $x_i = iL_x/N_x (0 \le i \le N_x)$ and $y_j = jL_y/N_y (0 \le j \le N_y)$, and are stretched in the wall-normal direction with $z_k = \cos[\pi k/(N_z - 1)] (0 \le k \le N_z - 1)$. $(N_x \times N_y \times N_z)$ grid points are used in the computational box of size $L_x \times L_y \times 2$.

Time advance is achieved with a third-order Runge–Kutta method for the convective term and the Crank–Nicolson method for the pressure and viscous terms. An implicit treatment is employed to avoid extremely small time steps in the near wall region resulting from the Chebyshev discretization. De-aliasing via the "3/2 rule" has been applied to the nonlinear convective term. More details on the method can be found in [14,15,18,19].

B. DNS Cases and Results

Simulations have been carried out for turbulent channel flow at a series of Reynolds numbers up to $Re_\tau = 1440$. Large boxes have been used for each case to include the large scale structures in the computational domain. This is checked by making sure that the two-point correlation functions for velocity and pressure drop to zero at large separation [14,15]. In the x and y directions, resolutions are kept the same in wall units for all calculations, at $\Delta x^+ = 16.88$ and $\Delta y^+ = 8.44$ (the $Re_\tau = 130$ case has slightly lower values); these values are comparable to those used by KMM [9]. In the wall-normal direction more than 10 points are located in the near wall region $z^+ < 9$, with the first point 0.12 to 0.03 wall units from the wall. The grid spacing at the channel centerline increases from 4.71 wall units for $Re_\tau = 90$ to 9.42 for $Re_\tau = 1440$. For higher Reynolds number cases, it is comparable to Δy^+ but still lower than Δx^+. Computational parameters for each case are given in Table 1.

The initial flowfield used to start the simulation consisted of a base mean flow calculated from the log law, with sinusoidal velocity perturbations added. It was marched sufficiently far in time until the flow became fully developed, before any statistics were collected. This was monitored by comparing statistics from successive time segments; data from earlier segments were discarded if they showed a trend. Whenever an existing flowfield was available from either a coarse grid simulation or another (lower) Reynolds number case, it was interpolated in wave space to speed up the initial flow development.

After the flow had reached a statistically stable state, single-point and two-point statistics were collected for velocity, pressure, and their derivatives, including velocity moments up to fourth order. Details of quantities collected are given in Hu and Sandham [20]. Samples of the statistics are available at http://www.dnsdata.afm.ses.soton.ac.uk/. Data have been compared with KMM [9] and MKM [10], good agreement being found [14,15] for the corresponding (or nearest) Reynolds number case. Some mean flow quantities are given in Table 1. $U_{\max}$ and U_m are the channel centerline and mean velocity, respectively. δ_1 and θ are the boundary-layer displacement and momentum thickness on the channel walls. The calculated Reynolds number, based on friction velocity results calculated from mean velocity statistics, is close to the nominal value given for each simulation; the largest discrepancy (for the $Re_\tau = 1440$ case) is 0.78%, which is an indication of the quality of the statistics.

From measurements of Poiseuille flow in a high aspect ratio duct, Dean [21] concluded that the difference between centerline velocity and mean velocity $((U^*_{\max} - U^*_m)/u^*_\tau)$ in plane Poiseuille flow decreases with Reynolds number and tends to a constant value 2.64 for high Reynolds number ($Re_m = 2h^*U^*_m/\nu^* > 10^5$). This quantity ranges from 2.52 to 3.05 for the current calculations, with the lowest Reynolds number case ($Re_m = 2.57 \times 10^3$) having the highest value of 3.05; the others vary between 2.52 and 2.71 and show no clear trend with Reynolds number. The ratio $U_{\max}/U_m$ for the current simulations matches Dean's empirical formula $U_{\max}/U_m = 1.28Re_m^{-0.0116}$ to within 0.4% for $Re_\tau \ge 180$; the difference is 1% for $Re_\tau = 130$ and 4% for $Re_\tau = 90$.

Mean velocity profiles for each of the different Reynolds number cases are shown in Fig. 1. Viscous scaling is used for Fig. 1a, with velocity $u^+ = u^*/u^*_\tau$ plotted against distance from the wall in wall units, $z^+ = (h^* - |z^*|)u^*_\tau/\nu^*$. Velocity profiles collapse in the near wall region. Away from the wall, the three low Reynolds number cases ($Re_\tau = 180$, 130, 90) are influenced by the low Reynolds number effect noted in MKM [10], but the two cases with $Re_\tau = 360$ and 720 collapse up to $z^+ = 100$. Outer scaling is used for Fig. 1b, where the mean velocity normalized by the channel centerline velocity, $u/U_{\max}$, is plotted against distance from the wall, $z_w = 1 - |z|$. The collapsed region extends further towards the wall for higher Reynolds numbers, with the two highest Reynolds number cases showing collapse down to $z_w = 0.1$.

Figure 2 shows profiles of the rms velocities. There is a general trend for all three components to increase as the Reynolds number increases. The maximum streamwise rms velocity appears at $z^+ = 15$ for all Reynolds numbers. Changes in this maximum value with

Table 1 Parameters and mean flow properties for each simulation

Re_τ Nom.	Re_τ Calc.	Box size $(L_x \times L_y \times L_z)$	Grid points $(N_x \times N_y \times N_z)$	$U_{\max}$	U_m	δ_1	$\theta(\times 10^2)$
1440	1451.3	$12 \times 6 \times 2$	$1024 \times 1024 \times 481$	23.83	21.12	0.1135	8.557
720	716.5	$12 \times 6 \times 2$	$512 \times 512 \times 321$	21.52	18.93	0.1198	8.713
360	361.8	$12 \times 6 \times 2$	$256 \times 256 \times 161$	19.94	17.40	0.1273	8.720
180	180.2	$24 \times 12 \times 2$	$256 \times 256 \times 121$	18.20	15.66	0.1400	8.621
130	130.0	$24 \times 12 \times 2$	$196 \times 196 \times 81$	17.65	15.01	0.1496	8.646
90	90.0	$48 \times 24 \times 2$	$256 \times 256 \times 61$	17.29	14.25	0.1763	9.152

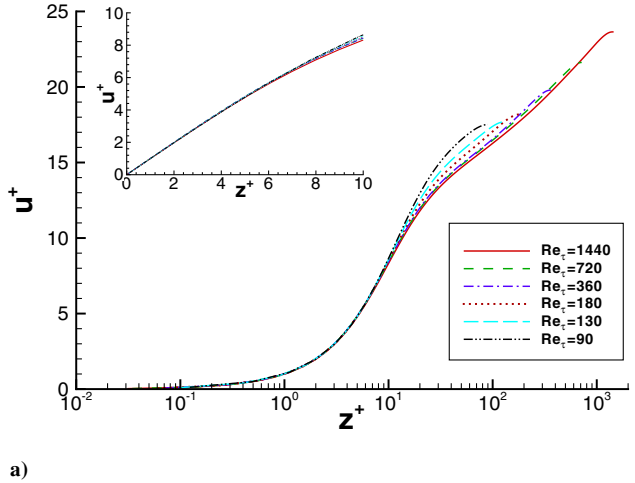

a)

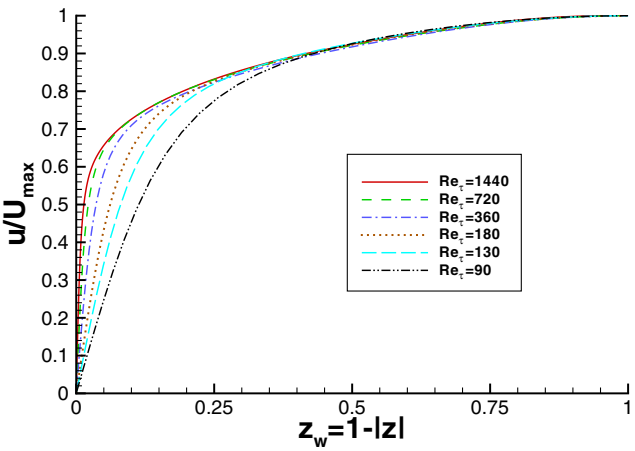

b)

Fig. 1 Mean velocity profiles for different Reynolds numbers. a) Viscous scaling; b) outer scaling.

Reynolds number are not as large as the corresponding changes in the other two components. The values are consistent with 2.70 ± 0.09 given by Mochizuki and Nieuwstadt [22], based on a survey of measurements in channel and pipe flows over the Reynolds number range of $Re_\tau = 100 \sim 4300$. Antonia and Kim [23] found from channel flow DNS data at $Re_\tau = 180$ and 400 that the variations of fluctuation velocities are much smaller if scaled on wall Kolmogorov scales. A similar trend has also been obtained from current data (not shown here) with the best collapse obtained for the wall-normal velocity in the near wall region. Variations in the other two components are smaller than using inner scaling for the near wall region, but no convincing collapse of current data has been found.

The statistics collected from the DNS allow calculation of all the terms in the transport equations for kinetic energy and Reynolds stresses. An example of the budget for turbulent kinetic energy is shown in Fig. 3 for $Re_\tau = 1440$. The imbalance is less than 5×10^{-4} (as shown in the inset plot), which is 3 orders of magnitude smaller than the maximum of the production term.

III. Spectra of Wall Pressure and Shear Stress from DNS

A. Wave-Number–Frequency Spectrum

After the flow has reached a fully developed state, time histories of the wall pressure and wall shear stresses (streamwise τ_x and spanwise τ_y) on both channel walls are collected for each streamwise and spanwise wave number. A typical time history is denoted below by $\tilde{q}(k_{xl}, k_{ym}, t_r)$. Each wave-number component is time Fourier

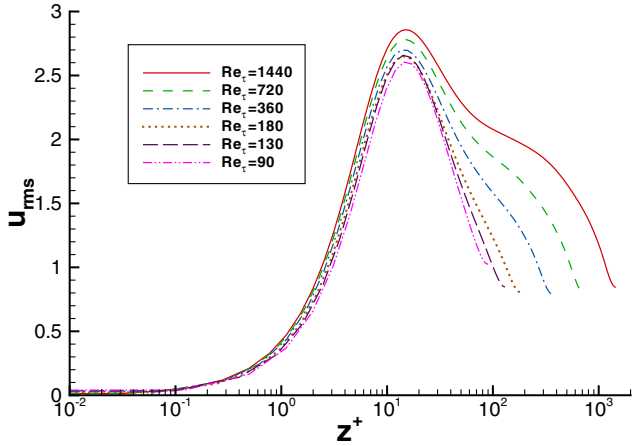

a)

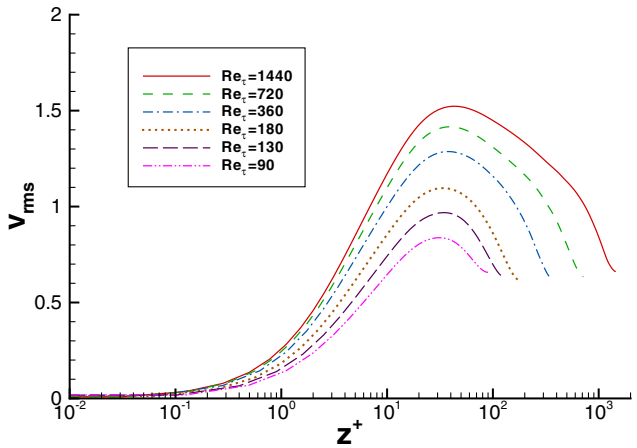

b)

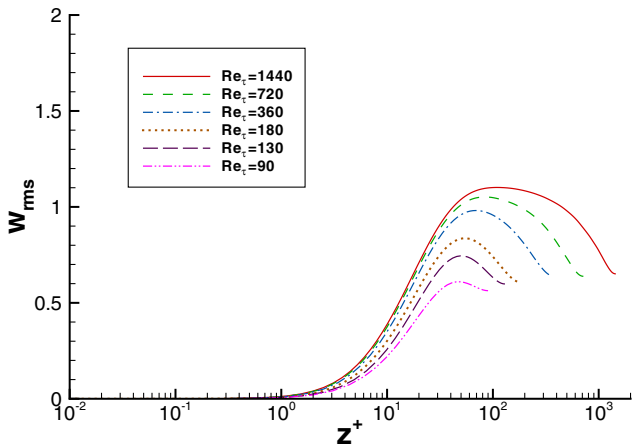

c)

Fig. 2 Profiles of rms velocity fluctuations for different Reynolds number. a) Streamwise, b) spanwise, and c) wall-normal component.

transformed by

$$\hat{q}(k_{xl}, k_{ym}, f_s) = \frac{1}{N} \sum_{r=0}^{N-1} \tilde{q}(k_{xl}, k_{ym}, t_r) e^{i2\pi rs/N} \tag{5}$$

Here t_r is the discrete sample time, given by $t_r = r\Delta t$, where Δt is the sampling time interval, and f_s is the nondimensional frequency $f_s = s/(N\Delta t)$, with $0 \le s \le N/2$ (r and s are integers). The number of samples N is even.

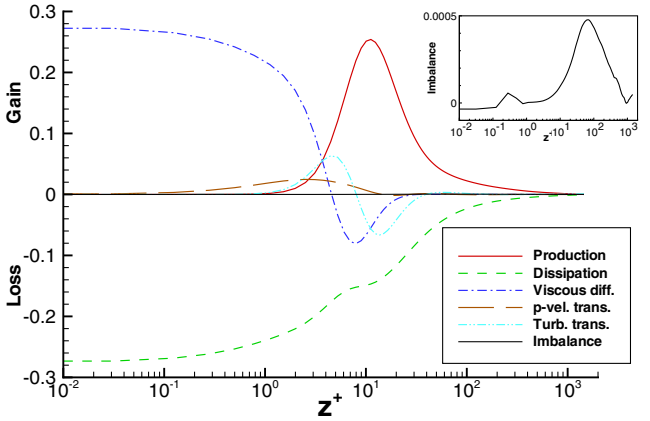

Fig. 3 Turbulent kinetic energy budget for $Re_\tau = 1440$. All quantities are scaled by u_τ^{*4}/ν^*.

The two-sided wave-number–frequency spectrum for wall pressure or wall shear stresses, $S_q(k_{xl}, k_{ym}, f_s)$, is defined as the following mathematical expectation, averaged over a large box $(L_x \times L_y)$ and a long sample (duration $T = N\Delta t$):

$$S_q(k_{xl}, k_{ym}, f_s) = E\left\{\lim_{L_x,L_y,T\to\infty} \frac{\hat{q}\hat{q}^\star}{(2\pi)^2 L_x L_y T}\right\} \tag{6}$$

The factor of $(2\pi)^{-2}$ is due to the use of wave-number components k_x, k_y rather than spatial frequencies. It should be mentioned that the sign convention used here for time Fourier transformation differs from the usual mathematical convention. The time transform is defined so that waves with the same sign of streamwise wave number and frequency travel with the flow, and waves with opposite signs travel against the flow.

To improve the quality of the spectral estimates, the time record is split into N_{seg} time segments with 50% overlap. Wave-number–frequency spectra are calculated for each time segment and averaged over all the time segments to give a smoother spectrum. Table 2 gives the sampling time interval Δt, total time record length T, total number of samples N, and number of time segments N_{seg} for each DNS case. By computing the time-segment average, a smoother spectrum is obtained although the shortened time record length for each segment reduces the frequency range of the spectrum at the low end. The frequency range for each case is also listed in Table 2.

Before a Fourier transform is taken of each time segment, the mean value of the signal is subtracted and a Hanning window is applied to the signal; therefore a factor of 8/3 has to be applied to the wave-number–frequency spectrum estimated from Eq. (6), to compensate for the Hanning window. Details on windowing can be found in signal processing textbooks, for example, Oppenheim et al. [24].

B. Point Spectrum

To compare the DNS results with the spectrum measured by a single-point transducer $G_T(\omega)$ ($\omega = 2\pi f$ is the angular frequency) in experiments [2–4,25], the wave-number–frequency spectrum, $S_q(k_x, k_y, f)$, calculated from (6) is integrated to get the one-sided ($\omega > 0$) point spectrum $G_T(\omega)$ as defined in Lauchle and Daniels [25]:

$$G_T(\omega) = \frac{1}{\pi} \iint S_q(k_x, k_y, f)\mathrm{d}k_x\mathrm{d}k_y \tag{7}$$

The factor $1/\pi$ is the result of the one-sided spectrum definition for $G_T(\omega)$ plus the use of frequency f rather than the angular frequency ω in Eq. (6).

IV. Wall-Pressure Spectrum

Record length, sampling interval, and other parameters for fluctuating wall pressure are given in Table 2 for each DNS case. Wave-number–frequency spectra of wall pressure are calculated for the cases listed in Table 1, using Eq. (6) together with the time-segment averaging technique given in the previous section. Examples have previously been presented in Hu et al. [14] for the lower Reynolds number cases ($Re_\tau \leq 360$) to study the low-wave-number region, for which contradictory predictions have been obtained from theoretical work [26,27]. This is important for structural vibrations and sound radiation produced by a turbulent boundary layer, as they are dominated by the subconvective wave-number (wave number less than the convective peak value) wall-pressure spectrum. Wall-pressure spectra obtained from DNS with large computational boxes were found to have nonzero low-wave-number limits [14]. DNS results from the higher Reynolds number cases presented here confirm this earlier finding. Here we present integrated point spectra as defined in (7).

In experimental studies of wall-pressure fluctuations under a turbulent boundary layer, various combinations of scaling variables have been used to collapse the measured point spectrum [2–4,28]. The goal is to find a similarity relation between different Reynolds number results, which in turn could lead to an empirical or semiempirical model for the wall-pressure spectrum. Viscous scaling, using τ_w^*, u_τ^*, and ν^*/u_τ^* as pressure, velocity, and length scales, is generally used to collapse the high-frequency end as it is believed that turbulent velocity fluctuations in the near wall region of the boundary layer contribute to this part of the wall-pressure spectrum. The low-frequency end is believed to result from turbulent velocity fluctuations across the entire boundary layer; therefore outer scaling, using freestream dynamic pressure, freestream velocity, and boundary-layer thickness as pressure, velocity, and length scales, is used for low frequencies. Different mixed scaling combinations of outer flow variables with viscous variables have been used for the midfrequency range.

Point spectra of wall pressure have been calculated using Eq. (7) together with DNS generated wave-number–frequency spectra. To reduce the disk space required to store the time series of wall quantities for all wave numbers, a sampling interval of every 20 time steps is used for the 1440 case compared to every 5 time steps for all other cases. This allows longer time record of the wall quantities being stored, from which spectra at lower frequency can be calculated. The sacrifice of the high-frequency range of spectra for low frequency is made as the Reynolds number scaling of wall-pressure spectra at the high-frequency end is relatively better understood than at the low-frequency end.

Wall-pressure spectra are shown in Fig. 4 in frequency-weighted form for each DNS case. Plotting the spectra in this premultiplied form has two advantages: first the premultiplied spectrum shows the energy contained in proportional (dimensionless) frequency bands; second in this plot the vertical axis is scaled by the square of a reference pressure and the horizontal axis by (the inverse of) a

Table 2 Sampling parameters

Re_τ Nom.	$Re = 2h^* U_{\max}^*/\nu^*$	Sampling Δt	Record length T	No. of samples	N_{seg}	Frequency range
1440	6.86×10^4	0.002	2.126	1063	7	$1.935 \leq f \leq 250$
720	3.08×10^4	0.00125	5.15	4120	7	$0.781 \leq f \leq 400$
360	1.45×10^4	0.0025	25.6	10240	9	$0.195 \leq f \leq 200$
180	6.55×10^3	0.01	82	8200	7	$0.0488 \leq f \leq 50$
130	4.59×10^3	0.0125	102.5	8200	7	$0.0390 \leq f \leq 40$
90	3.11×10^3	0.025	205	8200	7	$0.0195 \leq f \leq 20$

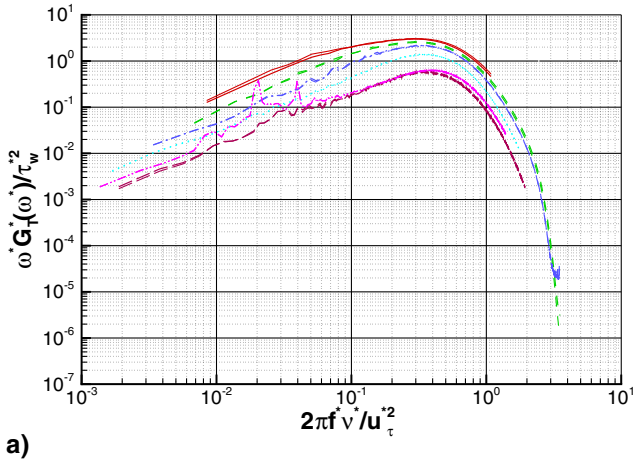

a)

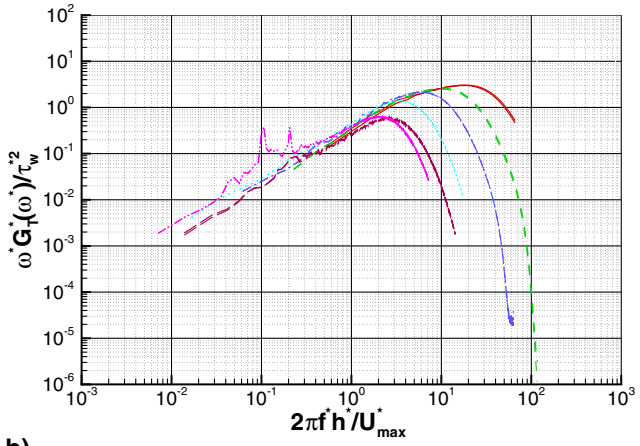

b)

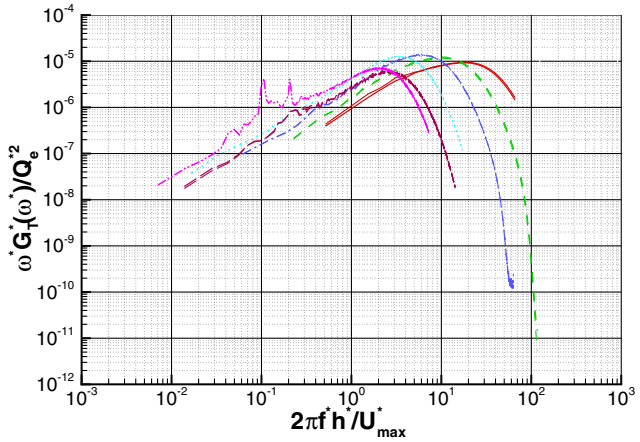

c)

Fig. 4 Point spectra of wall pressure from DNS plotted under different combinations of scaling variables. Solid lines: $Re_\tau = 1440$; dashed lines: $Re_\tau = 720$; dash-dotted lines: $Re_\tau = 360$; dotted lines: $Re_\tau = 180$; long-dashed lines: $Re_\tau = 130$; dash-double-dotted lines: $Re_\tau = 90$. Two lines are plotted for the two channel walls for each case, with a thick line for the upper wall and a thin line for the lower wall. a) Viscous scaling; b) mixed scaling; c) outer scaling.

reference time, making it easier to find the proper combination of reference variables to collapse the spectrum. For each DNS case, spectra for the two channel walls have been plotted with thick and thin lines. Agreement of data from the two walls provides a check on the convergence of the data sampling technique.

Viscous scaling, namely, τ_w^* as pressure scale and ν^*/u_τ^{*2} as time scale, is used in Fig. 4a to plot the frequency-weighted point spectra

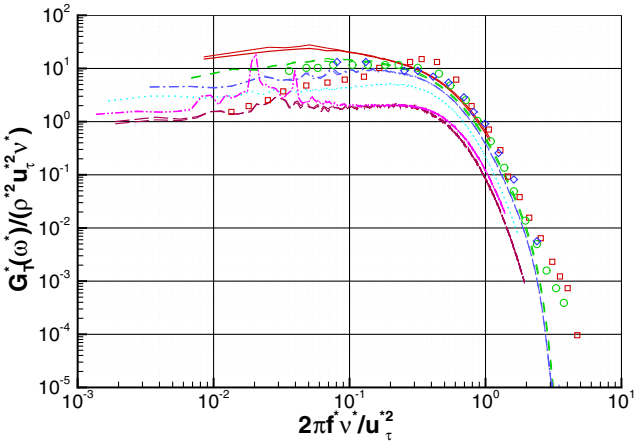

Fig. 5 Frequency-weighted point spectrum of wall pressure compared with experiments. Symbols are ○ for $Re_\theta = 1120$ channel flow data of Brungart et al. [4], □ for $Re_\theta = 1400$ pipe flow data of Lauchle and Daniels [25], and ◇ for $Re_\theta = 1400$ boundary-layer data of Schewe [1]. The present channel flow simulation for $Re_\tau = 720$ has $Re_\theta = 1343$. For line codes, see Fig. 4.

from each DNS case. The spectra plotted in this form show a peak, and the maximum energy appears at nondimensional angular frequency $\omega^+ = 2\pi f^* \nu^*/u_\tau^{*2} = 0.3$ for the three highest Reynolds numbers ($Re_\tau \geq 360$). Under viscous scaling the spectra collapse within 2 dB for frequencies greater than the peak frequency, where the maximum energy appears. Spectra for the low Reynolds number cases are influenced by low Reynolds number effects as indicated in the velocity profiles.

Various combinations of reference variables have been tried to scale the low and midfrequency regions of the wall-pressure spectra. A mixed scaling using the inner variable, mean wall shear stress τ_w^*, as pressure scale and the outer variable, $h^*/U^*_{\max}$, as time scale is found to give the best result, as plotted in Fig. 4b. The frequency-weighted spectra for $Re_\tau \geq 360$ are found to follow the same trend (close to a power law with an exponent of $6/5$) just before reaching their maximum values where the spectra level off and decrease at high frequencies. As found in Fig. 4a, the frequency at which the frequency-weighted spectra reach their maximum scales on wall variables as $\omega^+ = 0.3$.

Use of outer scaling, with (twice) the dynamic pressure at the centerline $Q_e^* = \rho^* U^{*2}_{\max}$ as reference pressure and $h^*/U^*_{\max}$ as reference time, is shown in Fig. 4c; it provides no useful improvement in collapse.

The entire unsegmented time record has been used to extend the low-frequency range of the calculated point spectra for the three highest Reynolds number cases. The extended spectra (not shown here) give good collapse under the mixed scaling used in Fig. 4b, but again show no sign of collapse under outer scaling. Goody [28] found the available experimental data for higher Reynolds numbers ($1.4 \times 10^3 < Re_\theta < 2.34 \times 10^4$) collapsed under outer scaling for $2\pi f^* h^*/U^*_{\max} < 0.3$, in conflict with our results in Fig. 4c. However only limited experimental data are available for this frequency range. Three points were provided by the measurement of Farabee and Casarella [2] at frequencies around 0.01, and two points were obtained from the measurement of McGrath and Simpson [29] at frequencies near 0.1. Therefore Goody used a mixed scaling in his modeling of the wall-pressure spectrum, with wall shear stress instead of the dynamics pressure as pressure scale.

For the two lowest Reynolds number cases ($Re_\tau = 90, 130$), distinct peaks in the spectrum are seen. These occur at nondimensional frequencies $\omega^+ = 0.02$ and 0.04 for $Re_\tau = 90$ and at $\omega^+ = 0.03$ for $Re_\tau = 130$. They appear to be an artifact of the finite box length in the periodically specified streamwise direction. Based on the convection velocity of wall pressure given in Hu et al. [14] ($U_c = 0.819 U_{\max}$), it is found that the primary peak frequency corresponds to the convection of wall pressure across the box. For the $Re_\tau = 90$ case, the nondimensional frequency for convection across

the periodically specified computational box is equal to $\omega^+ = 2\pi f^* \nu^* / u_\tau^{*2} = 2\pi U_c / L_x Re_\tau = 0.02$. In the simulation both the fundamental frequency and its first harmonic appeared in the spectrum. This value equals 0.029 for the 130 case, where a much less pronounced peak is also observed in the spectrum. This phenomenon only occurs at low Reynolds number when turbulence exhibits a self-generation mechanism as has been found by Jimenez and Moin [30] and Hamilton et al. [31]. As large computational boxes ($L_x = 48$ for $Re_\tau = 90$ and $L_x = 24$ for $Re_\tau = 130$) were used for these simulations, the peaks appear at low frequencies, and contribute little to the rms pressure. For example, replacing the values in the $Re_\tau = 90$ spectrum for the points within the two peaks (3 points for the first peak and 7 points for the second) with linearly interpolated values from neighboring points brings the calculated rms wall pressure down from 1.14 to 1.10.

Figure 5 compares DNS data with measurements of wall-pressure spectra by Brungart et al. [4] for channel flow at $Re_\theta = 1120$, by Lauchle and Daniels [25] for fully developed pipe flow at $Re_\theta = 1400$, and by Schewe [1] for a boundary layer in nonaccelerating flow at $Re_\theta = 1400$. The current DNS cases have Reynolds numbers Re_θ (based on channel centerline velocity and momentum thickness) that range from 142 to 2959. It can be seen that DNS data for $Re_\tau = 720$ (plotted as a dashed line in the figure, with $Re_\theta = 1343$) compare well with the experimental data of Brungart et al. [4] and Schewe [1], but are higher especially at low frequency than the pipe flow data of Lauchle and Daniels [25]. A similar comparison was also presented in Fig. 11 of Hu et al. [14]; a correction factor of 8/3 should be applied to the three DNS cases ($Re_\tau = 360$, 180, and 90) plotted in that figure.

The rms fluctuating wall pressure $(p_{\rm rms})_w$ scaled by mean wall shear stress τ_w^* is plotted in Fig. 6 for the DNS cases listed in Table 1. The current data are consistent with the DNS results for channel flow of KMM [9] and MKM [10]. Experimental data from Farabee and Casarella [2], Lauchle and Daniels [25], Schewe [1], and Bull and Thomas [32] are also plotted for comparison. Our present DNS results fall within the scatter of the experimental data. Farabee and Casarella [2] concluded that the mean square wall-pressure fluctuation varies linearly with the logarithm of Reynolds number. A best fit to the current results and the DNS data of MKM [10] for $Re_\tau \geq 360$ gives the following formula, shown in Fig. 6 by a solid line:

$$(p_{\rm rms})_w^2 = 2.60\ \ell_n(Re_\tau) - 11.25 \tag{8}$$

The slope is steeper than that given by Farabee and Casarella [2], which is shown by a dash-dotted line in Fig. 6.

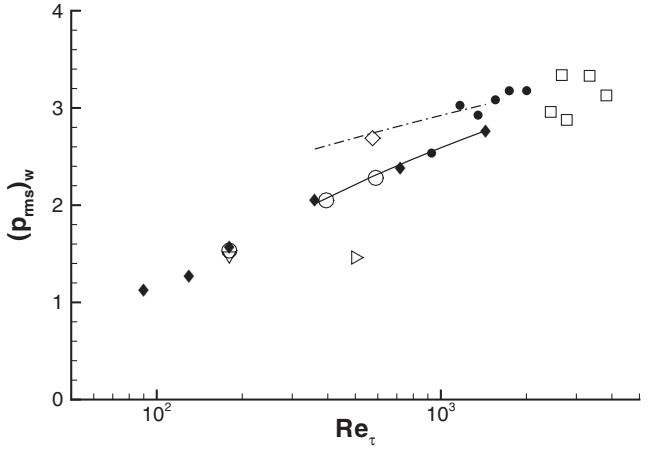

Fig. 6 DNS results of rms wall pressure (◆) compared with DNS of KMM [9] (▽) and MKM [10] (○), and with experiments of Farabee and Casarella [2] (●), Lauchle and Daniels [25] (▷), Schewe [32] (◇), and Bull and Thomas [32] (□). Solid line: best fit of DNS data, Eq. (8); dash-dotted line: formula of Farabee and Casarella [2].

V. Wall Shear Stress spectrum

Wave-number–frequency spectra and point spectra have been calculated for the fluctuating wall shear stress in the same way as for the wall pressure. Wave-number–frequency spectra of wall shear stresses for $Re_\tau \leq 360$ have been published in Hu et al. [14] with an emphasis on the low-wave-number behavior, which is the dominant dipole sources for sound radiation from wall-bounded turbulent flows at low Mach numbers [15]. It was found that the spectra for both streamwise and spanwise wall shear stresses have nonzero low-wave-number limits. Results for high Reynolds numbers from the current study also show nonzero low-wave-number limits, confirming the above conclusion.

Streamwise wall shear stress fluctuations have been measured by various investigators for wall-bounded turbulent flows [7,8,33–35]; the results are sensitive to the technique used in the experiment. For example, rms wall shear stresses obtained by flush-mounted hot films are significantly lower than from all other types of technique. Alfredsson et al. [7] compared available data on rms streamwise fluctuating wall shear stress measured with different calibration and acquisition techniques. They concluded that the large range of rms values obtained (0.06–0.4) is due to difficulties in measuring the velocity in the sublayer, and to the disturbance caused by the sensor in the flow. Methods that suffer less from these limitations tend to give a higher value. For example, the pulsed wire technique of Castro et al. [36] measured a value of 0.4 for their smallest probes.

The finite probe size is also a major source of experimental error. Willmarth and Sharma [37] found that hot wires longer than 30 wall units significantly underestimate the rms wall shear stress.

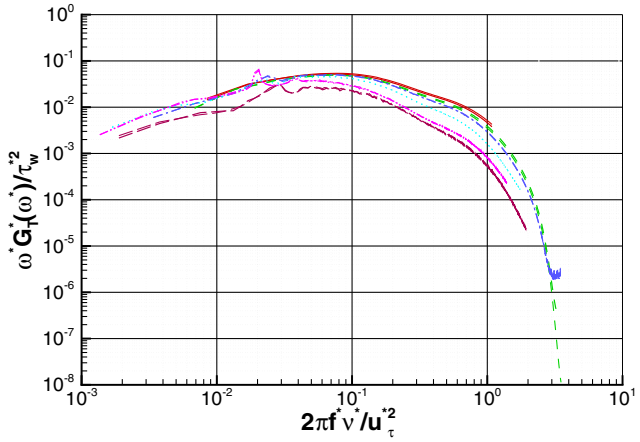

a)

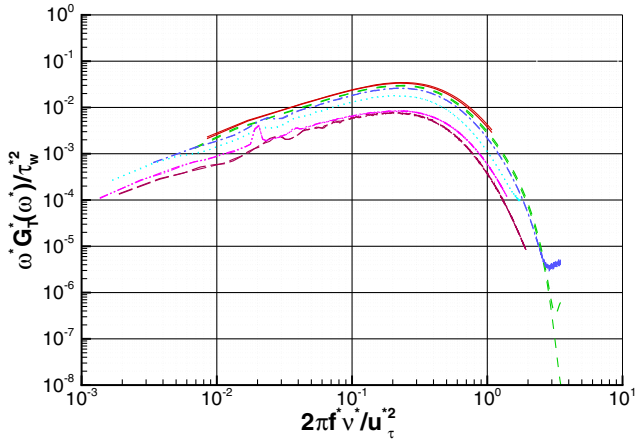

b)

Fig. 7 Frequency-weighted point spectra for wall shear stresses from DNS normalized by viscous variables: wall shear stress τ_w and viscous time scale ν^*/u_τ^{*2}. See Fig. 4 for line codes. a) Streamwise component; b) spanwise component.

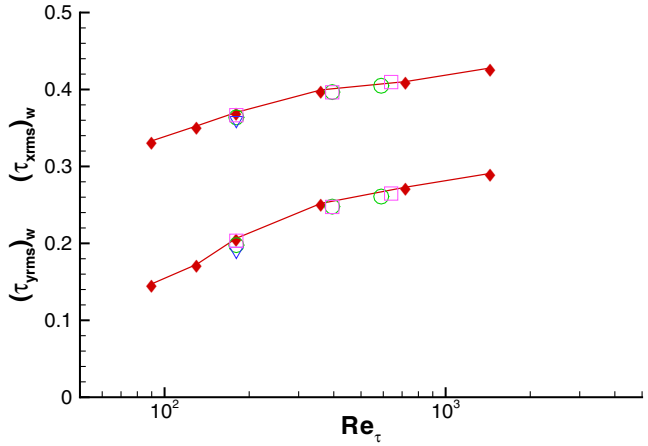

Fig. 8 The rms wall shear stresses calculated from DNS for channel flow. Solid diamonds with connecting lines: current results; ▽: DNS of KMM [9]; ○: DNS of MKM [10]; □: DNS of Abe et al. [16]. The upper line shows the streamwise component and the lower line shows the spanwise component.

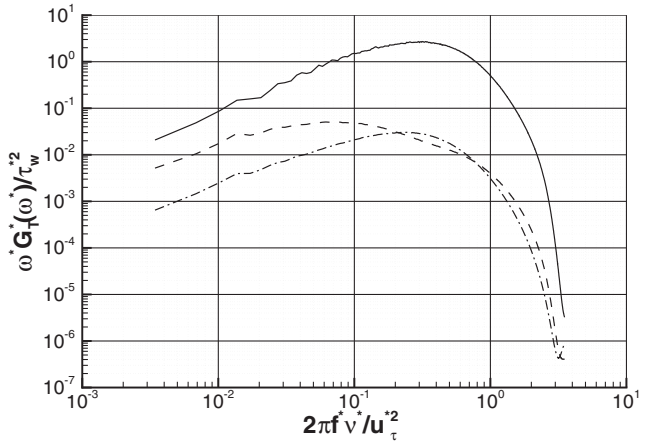

Fig. 9 Comparison of spectra for wall pressure (solid line), streamwise (dashed line), and spanwise (dash-dotted line) wall shear stresses at $Re_\tau = 720$.

Blackwelder and Haritonidis [38] found that only sensors smaller than 20 wall units were free from spatial averaging effects. It is difficult to find the best scaling for wall shear stress spectra from measured data due to experimental uncertainties [8]. Because the high resolution used in DNS gives more reliable results, data from DNS calculations have been used for experimental calibration; for example, Yoshino et al. [39] used channel flow DNS data to calibrate their experimental technique.

Point spectra for wall shear stress are shown in Fig. 7a for the streamwise component and in Fig. 7b for the spanwise component. Frequency-weighted point spectra are plotted using viscous scaling, with τ_w^* as reference shear stress and ν^*/u_τ^{*2} as reference time, as used in Fig. 4a for the wall-pressure spectrum. In each case two lines with different thickness are plotted, one for each channel wall. The spectra for both shear stress components collapse for the three DNS cases with $Re_\tau \geq 360$, within the current frequency range. The frequency-weighted spectra reach maximum at $\omega^+ = 0.075$ for the streamwise component and at a higher frequency of $\omega^+ = 0.23$ for the spanwise component, compared to a peak frequency of $\omega^+ = 0.3$ for the wall-pressure spectrum. Distinct peaks in the spectra for low Reynolds numbers appear at $\omega^+ = 0.02$ for $Re_\tau = 90$ and at $\omega^+ = 0.03$ for $Re_\tau = 130$; these peaks are an artifact of the finite box size, as explained in the previous section.

Figure 8 shows the rms values of both streamwise and spanwise fluctuating wall shear stresses normalized by the mean wall shear stress. Our current results show good agreement with the DNS data of KMM [9], MKM [10], and Abe et al. [16]. Taken together these DNS data show that, within the current Reynolds number range, the rms for the streamwise component is 1.5 to 2 times that for the spanwise component. The rms values increase with Reynolds number from 0.33 to 0.43 for the streamwise component, and from 0.15 to 0.29 for the spanwise component. However, the rate of increase is gradually reducing, and the current DNS data suggest some leveling off at high Reynolds number.

The wall-pressure spectrum is 7–20 dB (depending on frequency) higher than the spectrum for the streamwise wall shear stress, and 15–20 dB higher than that for the spanwise component. Those values are comparable to boundary-layer measurements at $Re_\theta = 8200$ and 13,400 by Keith and Bennett [8], who found that the wall-pressure spectrum is 18–24 dB higher than that of the streamwise wall shear stress. The spectra of the two shear stress components are virtually the same at frequencies above $\omega^+ = 0.23$ (the peak frequency of the frequency-weighted spectrum for the spanwise component) showing the homogeneity of wall shear stress at high frequencies, and the streamwise spectrum is about 10 dB higher at low frequencies. Typical results are shown in Fig. 9 for $Re_\tau = 720$.

Probability density functions (PDFs) $P(q')$ have been calculated for both fluctuating wall pressure and shear stress. The skewness $S(q') = \overline{q'^3}/\sigma^3$ (σ is the standard deviation for the fluctuating quantity q', taken to be its rms value) and the flatness $F(q') = \overline{q'^4}/\sigma^4$ are given in Table 3. The PDFs for the lowest Reynolds number, $Re_\tau = 90$, are clearly different. For $Re_\tau \geq 180$, there is a weak dependence on Reynolds number, illustrated in Fig. 10 for the fluctuating streamwise shear stress and in Fig. 11 for the fluctuating wall pressure. Data have been plotted on a linear scale to show the shape and Reynolds number trends, and on a logarithm scale to emphasize the tail region. Data from Sreenivasan and Antonia [33], Wietrzak and Lueptow [35], and Colella and Keith [40] are plotted for comparison together with a Gaussian profile for reference.

It is noticed that for the current fully developed turbulent channel flows, which are under weak favorable pressure gradients, the probability of negative streamwise shear stress occurring at the wall is not zero (the vertical bars in Fig. 10b mark positions for $\tau_x = 0$); the probability increases with Reynolds number from 3.00×10^{-5} at $Re_\tau = 90$ to 8.54×10^{-4} at $Re_\tau = 1440$. The occurrence of negative shear stress has also been noted by Spalart and Coleman [41] for the zero pressure gradient turbulent boundary-layer simulation of Spalart [42].

The PDF for the streamwise shear stress is skewed with its maximum appearing at $\tau_x' = -0.55\sigma$. The skewness is around 1, compared to experimental results of 0.80 by Wietrzak and Lueptow [35] for axisymmetric boundary layer at $Re_\theta = 3050$, 0.66 to 0.73 by Castro et al. [36] for a flat plate boundary layer with $Re_\theta = 815$ to 1202, and 1.00 by Alfredsson et al. [7] for channel and boundary-layer flow. The wall-pressure PDFs are symmetric as has been found by Lamballais et al. [43] in their channel flow DNS study and are weakly Reynolds number dependent for $Re_\tau \geq 180$.

Figure 12 shows all the PDFs for $Re_\tau = 1440$; the Gaussian distribution is also plotted for comparison. The PDFs for wall pressure and spanwise wall shear stress are symmetric (their skewnesses are of the order of 10^{-2}). All the PDFs show higher peaks than the Gaussian distribution, consistent with the high flatness factors given in Table 3 (Gaussian flatness = 3); the flatness for τ_y' is nearly double that for τ_x'.

Table 3 Flatness and skewness factors

Re_τ	$F(p')$	$S(\tau_x')$	$F(\tau_x')$	$F(\tau_y')$	Probability for $\tau_x < 0$
1440	5.66	1.09	5.33	10.25	8.54×10^{-4}
720	5.65	1.02	4.97	9.57	6.23×10^{-4}
360	5.59	0.99	4.75	8.97	4.36×10^{-4}
180	5.56	0.96	4.42	8.43	1.35×10^{-4}
90	7.54	1.14	5.77	12.83	3.00×10^{-5}

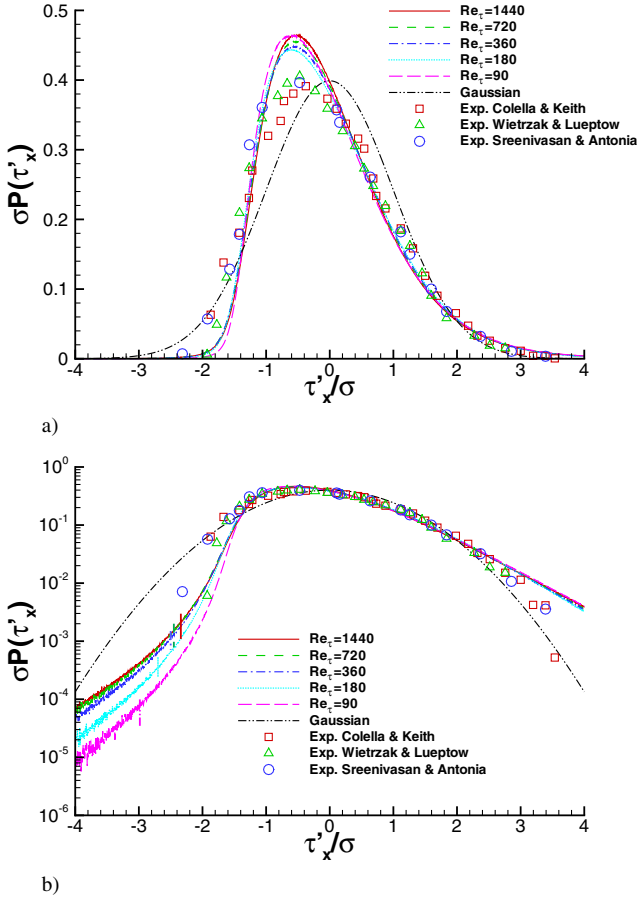

Fig. 10 PDFs for the streamwise wall shear stress at different Reynolds numbers plotted on a linear scale a) and logarithmic scale b) to emphasis the nonzero tails for $\tau_x < 0$. Lines for $Re_\tau = 1440$ and 720 overlapping each other. Vertical bars in b) mark positions for $\tau_x = 0$.

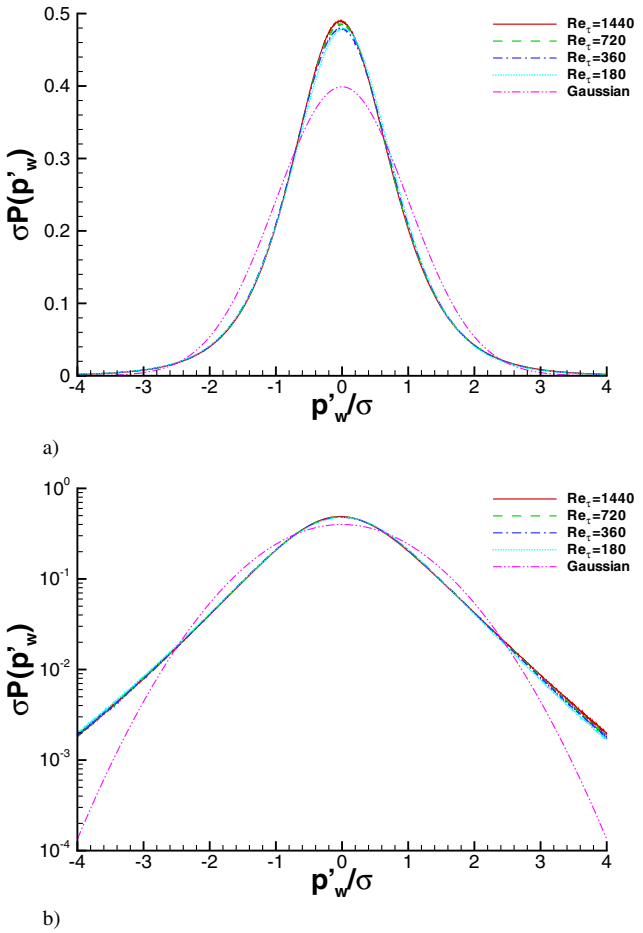

Fig. 11 PDFs for wall-pressure fluctuations at different Reynolds numbers plotted on a linear scale a) and logarithmic scale b). Gaussian profile is also plotted for comparison.

VI. Conclusions

Wall pressure and wall shear stress spectra have been obtained from DNS of turbulent plane channel flow at a series of Reynolds numbers up to $Re_\tau = 1440$. Wall-pressure spectra have been compared with experiments, showing good agreement for similar Reynolds numbers. It is found that a mixed scaling (with τ_w^*, centerline velocity $u_{\max}^*$, and channel half-width h^* as pressure, velocity, and length scales) collapses the wall-pressure spectra for $Re_\tau \geq 360$ in the low-frequency range below the peak of the frequency-weighted spectrum. Above the peak frequency, wall-pressure spectra collapse under viscous scaling. Wall shear stress spectra are found to collapse under viscous scaling over the whole frequency range for $Re_\tau \geq 360$. The point spectrum of wall pressure is generally higher than that of the wall shear stress components. The spectra for the two shear stress components are virtually the same at scaled frequencies above 0.23, whereas the streamwise spectrum is higher by up to 10 dB at lower frequencies. The scaled mean square wall-pressure fluctuation is found to increase linearly with the logarithm of Reynolds number, a best fit of the DNS results for $Re_\tau \geq 360$ giving a steeper slope than Farabee and Casarella's [2] formula derived from experimental data. The scaled rms wall shear stresses also increase with Reynolds number, ranging from 0.33 to 0.43 for the streamwise component and from 0.15 to 0.29 for the spanwise component. However the rate of increase is gradually diminishing over the present range of Re_τ, suggesting some leveling off at high Reynolds number.

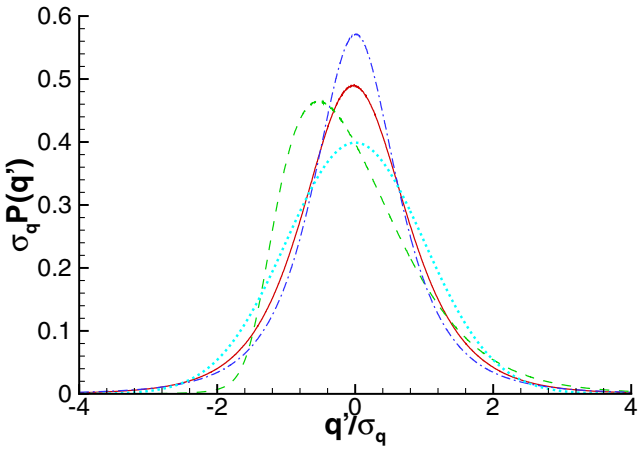

Fig. 12 Comparison of PDFs for wall pressure (solid line), streamwise (dashed line), and spanwise (dash-dotted line) wall shear stresses at $Re_\tau = 1440$ with Gaussian distribution (dotted line).

Acknowledgements

This study was supported by the Engineering and Physical Sciences Research Council (EPSRC), U.K. under Grant GR/M38865. Supercomputer time for the DNS calculations was also provided by the U.K. Turbulence Consortium under EPSRC Grants GR/M08424 and GR/R 64964. The $Re_\tau = 1440$ simulation was monitored by R. Johnstone of Daresbury Laboratory, Council for the Central Laboratory of the Research Councils, U.K. The authors are grateful to I. P. Castro and G. N. Coleman of the University of Southampton for their useful discussions.

References

[1] Schewe, G., "On the Structure and Resolution of Wall-Pressure Fluctuations Associated with Turbulent Boundary-Layer Flow," *Journal of Fluid Mechanics*, Vol. 134, Nov. 1983, pp. 311–328.

[2] Farabee, T. M., and Casarella, M. J., "Spectral Features of Wall Pressure Fluctuations Beneath Turbulent Boundary Layers," *Physics of Fluids A*, Vol. 3, No. 10, 1991, pp. 2410–2420.

[3] Keith, W. L., Hurdis, D. A., and Abraham, B. M., "A Comparison of Turbulent Boundary Layer Wallpressure Spectra," *Transactions of the ASME: Journal of Fluids Engineering*," Vol. 114, Sept. 1992, pp. 338–347.

[4] Brungart, T. A., Lauchle, G. C., Deutsch, S., and Riggs, E. T., "Outer-Flow Effects on Turbulent Boundary Layer Wall Pressure Fluctuations," *Journal of the Acoustical Society of America*, Vol. 105, No. 4, 1999, pp. 2097–2106.

[5] Goody, M. C., and Simpson, R. L., "Surface Pressure Fluctuations Beneath Two- and Three-Dimensional Turbulent Boundary Layers," *AIAA Journal*, Vol. 38, No. 10, 2000, pp. 1822–1831.

[6] Löfdahl, L., "MEMS Sensors for Turbulence Measurements and Flow Control," *Proceedings of the Third International Symposium on Turbulence and Shear Flow Phenomena*, edited by N. Kasagi, J. K. Eaton, R. Friedrich, J. A. C. Humphrey, M. A. Leschziner, and T. Miyauchi, June 2003, pp. 25–27.

[7] Alfredsson, P. H., Johansson, A. V., Haritonidis, J. H., and Eckelmann, H., "The Fluctuating Wall-Shear Stress and the Velocity Field in the Viscous Sublayer," *Physics of Fluids*, Vol. 31, No. 5, 1988, pp. 1026–1033.

[8] Keith, W. L., and Bennett, J. C., Jr., "Low-Frequency Spectra of the Wall Shear Stress and Wall Pressure in a Turbulent Boundary Layer," *AIAA Journal*, Vol. 29, No. 4, 1991, pp. 526–530.

[9] Kim, J., Moin, P., and Moser, R., "Turbulence Statistics in Fully Developed Channel Flow at Low Reynolds Number," *Journal of Fluid Mechanics*, Vol. 177, April 1987, pp. 133–166.

[10] Moser, R. D., Kim, J., and Mansour, N. N., "Direct Numerical Simulation of Turbulent Channel Flow up to $Ret = 590$," *Physics of Fluids*, Vol. 11, No. 4, 1999, pp. 943–945.

[11] Del Alamo, J. C., Jimenez, J., Zandonade, P., and Moser, R. D., "Scaling of the Energy Spectra of Turbulent Channels," *Journal of Fluid Mechanics*, Vol. 500, 10 Feb. 2004, pp. 135–144.

[12] Choi, H., and Moin, P., "On the Space-Time Characteristics of Wall-Pressure Fluctuations," *Physics of Fluids A*, Vol. 2, No. 8, 1990, pp. 1450–1460.

[13] Jeon, S., Choi, H., Yoo, J. Y., and Moin, P., "Space-Time Characteristics of Wall Shear-Stress Fluctuations in a Low-Reynolds-Number Channel Flow," *Physics of Fluids*, Vol. 11, No. 10, 1999, pp. 3084–3094.

[14] Hu, Z. W., Morfey, C. L., and Sandham, N. D., "Aeroacoustics of Wall-Bounded Turbulent Flow," *AIAA Journal*, Vol. 40, No. 3, 2002, pp. 465–473.

[15] Hu, Z. W., Morfey, C. L., and Sandham, N. D., "Sound Radiation in Turbulent Channel Flows," *Journal of Fluid Mechanics*, Vol. 475, 25 Jan. 2003, pp. 269–302.

[16] Abe, H., Kawamura, H., and Choi, H., "Very Large-Scale Structures and Their Effects on the Wall Shearstress Fluctuations in a Turbulent Channel Flow up to $Re = 640$," *Transactions of the ASME: Journal of Fluids Engineering*, Vol. 126, No. 9, 2004, pp. 835–843.

[17] Kleiser, L., and Schumann, U., "Treatment of Incompressibility and Boundary Layer Conditions in 3D Numerical Spectral Simulations of Plane Channel Flows," *Proceedings of the 3rd GAMM Conference on Numerical Method in Fluid Mechanics*, edited by E. H. Hirschel, Vieweg, Brunswick, Germany, 1980, pp. 165–173.

[18] Canuto, C., Hussaini, M. Y., Quarteroni, A., and Zang, T. A., *Spectral Methods in Fluid Dynamics*, Springer–Verlag, New York, 1987.

[19] Sandham, N. D., and Howard, R. J. A., "Direct Simulation of Turbulence Using Massively Parallel Computers," *Parallel Computation Fluid Dynamics*, edited by D. R. Emerson, A. Ecer, J. Periaux, N. Satofuka, and P. Fox, Elsevier, New York, 1998, pp. 23–32.

[20] Hu, Z. W., and Sandham, N. D., "DNS Databases for Turbulent Couette and Poiseuille Flow," TR AFM-01/04, AFM Research Group, School of Engineering Sciences, University of Southampton, Aug. 2001.

[21] Dean, R. B., "Reynolds Number Dependence of Skin Friction and Other Bulk Flow Variables in Two-Dimensional Rectangular Duct Flow," *Transactions of the ASME: Journal of Fluids Engineering*, Vol. 100, June 1978, pp. 215–223.

[22] Mochizuki, S., and Nieuwstadt, F. T. M., "Reynolds-Number-Dependence of the Maximum in the Streamwise Velocity Fluctuations in Wall Turbulence," *Experiments in Fluids*, Vol. 21, 1996, pp. 218–226.

[23] Antonia, R. A., and Kim, J., "Low-Reynolds-Number Effects on Near-Wall Turbulence," *Journal of Fluid Mechanics*, Vol. 276, 10 Oct. 1994, pp. 61–80.

[24] Oppenheim, A. V., Schafer, R. W., and Buck, J. R., *Discrete-Time Signal Processing*, 2nd ed., Prentice Hall, New York, 1999.

[25] Lauchle, G. C., and Daniels, M. A., "Wall Pressure Fluctuations in Turbulent Pipe Flow," *Physics of Fluids*, Vol. 30, No. 10, 1987, pp. 3019–3024.

[26] Chase, D. M., "The Character of the Turbulent Wall Pressure Spectrum at Subconvective Wavenumbers and a Suggested Comprehensive Model," *Journal of Sound and Vibration*, Vol. 112, No. 1, 1987, pp. 125–147.

[27] Howe, M. S., "A Note on the Kraichnan–Phillips Theorem," *Journal of Fluid Mechanics*, Vol. 234, Jan. 1992, pp. 443–448.

[28] Goody, M. C., "Empirical Spectral Model of Surface Pressure Fluctuations," *AIAA Journal*, Vol. 42, No. 9, 2004, pp. 1788–1794.

[29] McGrath, B. E., and Simpson, R. L., "Some Features of Surface Pressure Fluctuations in Turbulent Boundary Layers with Zero and Favourable Pressure Gradients," NASA, CR-4051, 1987.

[30] Jimenez, J., and Moin, P., "The Minimum Flow Unit in Near-Wall Turbulence," *Journal of Fluid Mechanics*, Vol. 225, April 1991, pp. 213–240.

[31] Hamilton, J. M., Kim, J., and Walee, F., "Regeneration Mechanisms of Near-Wall Turbulence Structures," *Journal of Fluid Mechanics*, Vol. 287, 25 March 1995, pp. 317–348.

[32] Bull, M. K., and Thomas, A. S. W., "High Frequency Wall-Pressure Fluctuations in Turbulent Boundary Layers," *Physics of Fluids*, Vol. 19, No. 4, 1976, pp. 597–599.

[33] Sreenivasan, K. R., and Antonia, R. A., "Properties of Wall Shear Stress Fluctuations in a Turbulent Duct Flow," *Transactions of the ASME: Journal of Applied Mechanics*, Vol. 44, Sept. 1977, pp. 389–395.

[34] Shah, D. A., and Antonia, R. A., "Scaling of Wall Shear Stress Fluctuations in a Turbulent Duct Flow," *AIAA Journal*, Vol. 25, No. 1, 1987, pp. 22–29.

[35] Wietrzak, A., and Lueptow, R. M., "Wall Shear Stress and Velocity in a Turbulent Axisymmetric Boundary Layer," *Journal of Fluid Mechanics*, Vol. 259, Feb. 1994, pp. 191–218.

[36] Castro, I. P., Dianat, M., and Bradbury, L. J. S., "The Pulsed Wire Skin-Friction Measurement Technique," *Turbulent Shear Flows 5: Selected Papers from the Fifth International Symposium on Turbulent Shear Flows, 1985*, edited by F. Durst, B. E. Launder, J. L. Lumley, F. W. Schmidt, and J. H. Whitelaw, Springer–Verlag, Berlin, 1987, pp. 278–290.

[37] Willmarth, W. W., and Sharma, L. K., "Study of Turbulent Structure with Hot Wires Smaller than the Viscous Length," *Journal of Fluid Mechanics*, Vol. 142, May 1984, pp. 121–149.

[38] Blackwelder, R. F., and Haritonidis, J. H., "Scaling of the Bursting Frequency in Turbulent Boundary Layer," *Journal of Fluid Mechanics*, Vol. 132, July 1983, pp. 87–103.

[39] Yoshino, T., Suzuki, Y., Kasagi, N., and Kamiunten, S., "Assessment of the Wall Shear Stress Measurement with Arrayed Micro Hot-Film Sensors in a Turbulent Channel Flow," *Proceedings of the Second International Symposium on Turbulence Shear Flow Phenomena*, edited by E. Lindborg, A. Johansson, J. Eaton, J. Humphrey, N. Kasagi, M. Leschziner, and M. Sommerfeld, Vol. 2, 27–29 June 2001, pp. 153–158.

[40] Colella, K. J., and Keith, W. L., "Measurements and Scaling of Wall Shear Stress Fluctuations," *Experiments in Fluids*, Vol. 34, No. 2, 2003, pp. 253–260.

[41] Spalart, P. R., and Coleman, G. N., "Numerical Study of a Separation Bubble with Heat Transfer," *European Journal of Mechanics, B/Fluids*, Vol. 16, No. 2, 1997, pp. 169–189.

[42] Spalart, P. R., "Direct Simulation of a Turbulent Boundary Layer up to $Re = 1410$," *Journal of Fluid Mechanics*, Vol. 187, Feb. 1988, pp. 61–98.

[43] Lamballais, E., Lesieur, M., and Metais, O., "Probability Distribution Functions and Coherent Structures in a Turbulent Channel," *Physical Review E*, Vol. 56, No. 6, 1997, pp. 6761–6766.

C. Bailly
Associate Editor